JOURNAL OF SPACECRAFT AND ROCKETS
Vol. 46, No. 6, November–December 2009

Phoenix Landing Site Hazard Assessment and Selection

David A. Spencer, Douglas S. Adams, Eugene Bonfiglio, and Matthew Golombek
California Institute of Technology, Pasadena, California 91109
Raymond Arvidson
Washington University, St. Louis, Missouri 63130
and
Kim Seelos
Applied Physics Laboratory, Johns Hopkins University, Laurel, Maryland 20723

DOI: 10.2514/1.43932

The Phoenix Mars Scout landing site hazard assessment and selection process began with a survey of the latitude band from 65–72°N to identify candidate landing regions that were accessible, safe, and suitable for meeting the mission science objectives. Four candidate landing regions were identified based upon proximity of ground ice to the surface. Thermal inertia data, visible imagery, and topographic maps were combined to make an initial assessment of rock abundance and slopes. Broadly distributed high-resolution images enabled refined interpretation of the lower-resolution data sets. Based upon this assessment, a broad valley to the west of Heimdall crater at 68.3°N, 124.6°W was selected as the target landing region for the Phoenix mission. A detailed evaluation of this region resulted in the identification of eight different geologic units, with each unit exhibiting characteristic terrain type and rock abundances. Targeted high-resolution images were acquired across much of the region. An autonomous rock-counting algorithm was used to develop probabilistic risk distributions. Landing ellipse placement was selected to maximize the probability of a safe landing considering rock and slope hazards, including craters. Postlanding images from the Phoenix stereoscopic imager show a landing site generally devoid of hazardous rocks and slopes, consistent with predictions.

Introduction

THE Phoenix lander was designed to operate in the Mars latitude range of 65–72°N, with a 90-sol primary surface mission beginning in late northern spring (Mars solar longitude 76.6°) and continuing into summer. The Phoenix entry, descent, and landing system used a heat shield and parachute for deceleration from hypersonic to subsonic velocities, a Doppler RADAR to detect the surface and estimate the altitude and descent velocity, a set of 12 pulse-mode descent engines to slow the descent rate and allow the vehicle to reduce horizontal velocity to less than 1.4 m/s and vertical velocity to 2.4 ± 1.0 m/s at touchdown, and a landing system consisting of three lander legs, stabilizers, and shock absorbers. The landing site was constrained to surface elevations of −3.5 km or lower relative to the Mars Orbiter Laser Altimeter (MOLA) reference ellipsoid. The three-legged lander design was robust to surface slopes of up to 16 deg, but was susceptible to impact with rocks having heights of 0.5 m or greater [1]. Scenarios that could lead to a mission failure or degraded mission included tipover due to steep slopes, lander instability as a result of one or more lander leg being on a rock, rock impact penetrating the lander thermal enclosure, and solar array deployment failure due to obstruction from rocks or the ground itself. Each of these scenarios was evaluated as part of the landing risk assessment.

The Phoenix landing site selection process expanded upon approaches and tools developed for the Mars Exploration Rover (MER) mission [2]. Visible and infrared data sets from the Mars Odyssey Thermal Emission Imaging System (THEMIS) were combined with MOLA topographic data and visible images from the Mars Global Surveyor (MGS) Mars orbiting camera to assess the geologic structure of candidate landing sites and assess landing risks. Science prioritization within the latitude band resulted in four candidate landing regions [3] (regions A–D, shown in Fig. 1) selected for further study in 2004. These regions were considered to be attractive for mission science return based upon the modeled proximity of ground ice to the surface. The regions are 20° in longitude by 7° in latitude. Region B was initially favored based upon an expected soil overburden above the ice table of 10 cm or more. In September 2006, imaging by the Mars Reconnaissance Orbiter's High-Resolution Science Experiment (MRO HiRISE) at 0.31 m/pixel showed an abundance of rock fields throughout region B. The Phoenix landing site selection team renewed their search for a safe site, and supplemented the existing data sets with new HiRISE images. The team developed the capability to directly process the high-resolution images using algorithms that could identify and estimate the sizes of individual rocks. This autonomous rock-counting procedure represents a significant advancement in the landing site evaluation process beyond what was done for previous missions, allowing the hazards posed by rocks to be directly quantified. A campaign of detailed characterization using targeted high-resolution images along with existing thermal and visible data sets allowed the Phoenix landing site working group to identify an area within region D that had low rock abundances and benign surface slopes across a contiguous area that would allow the placement of a landing ellipse with a major axis of 100 km and a minor axis of 20 km.

The selected area within region D, identified as Box 1, is centered upon 68.25°N areocentric latitude, 126.25°W longitude. Box 1 dimensions are 2.5° in latitude and 8.5° in longitude. A defining feature within the region is Heimdall crater, located at 68.3°N, 124.6°W, approximately 10 km in diameter. A broad valley with generally low rock abundances extends to the west of Heimdall crater [4,5]. Statistical evaluation of the hazards to the landing system and subsequent solar array deployment formed the basis for landing ellipse placement within Box 1, and provided a quantitative assessment of the probability of landing success. This paper describes the geologic assessment of Box 1, details the quantitative landing hazard assessment, and describes the process of selecting the landing ellipse placement within Box 1. Summary conclusions are provided.

Received 19 February 2009; revision received 28 July 2009; accepted for publication 31 July 2009.

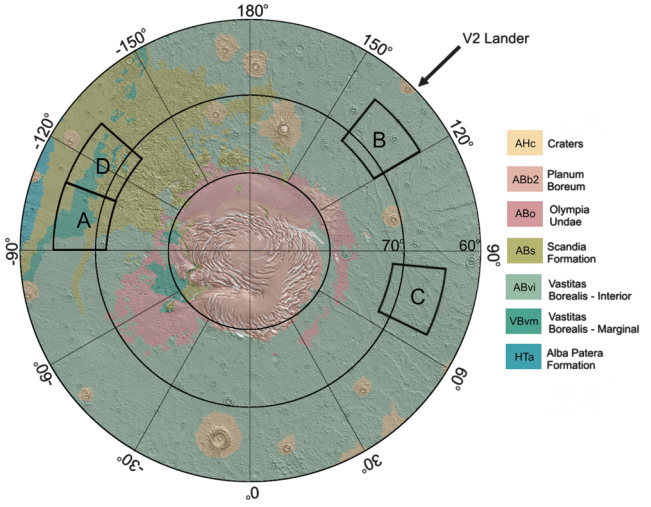

Fig. 1 Candidate landing regions within the 65–72°N latitude band [3].

Geologic Assessment

Prior work by Tanaka et al. [6] identified two geologic units spanning the region encompassed by Box 1: the Vastitas Borealis marginal unit and the Scandia formation (see Fig. 1). The Vastitas Borealis units are thought to be reworked volcanic and sedimentary deposits from both martian highland and lowland sources, and the marginal member of the Vastitas Borealis formation is described generally as a plains-forming unit with low plateaus. Landforms within the Vastitas Borealis formation suggest periglacial processes. The Scandia region unit overlies the Vastitas Borealis marginal unit and is characterized by widespread knobby terrain, mantled (sometimes layered) areas, and irregular topographic depressions. Mapping by Tanaka et al. [6] shows the Scandia region unit to be associated with the lower elevation valley portion of Box 1 as well as the southern, higher-elevation area that is dominated by knobs and hills. The Vastitas Borealis marginal unit appears exclusively associated with small flat-topped mesas and isolated plateaus.

Three remote sensing data sets were used by the Phoenix Landing Site Working Group in the determination of the geologic characteristics of Box 1. THEMIS visible data were mosaicked at 20 m/pixel and used in conjunction with MOLA topographic maps [7] (approximately 230 m/pixel) to create a consistent basemap across the region. Where available, 6 m/pixel MRO Context Imager data provided additional panchromatic information at enhanced spatial resolution. Geologic map units were characterized on the basis of topographic expression and albedo variations. Eight geologic units were identified [4,8] within the candidate landing site, as shown in Fig. 2. Broadly, the area is divided into two units, Highland and Lowland. The Highland unit occupies the southern portion of the region and exhibits a well-defined boundary with the topographically depressed Lowland unit. The vertical relief along the boundary ranges from 100 to 300 m across a horizontal distance of several kilometers, equating to mean slopes of less than 5 deg. The Lowland unit is divided into Bright and Dark subunits on the basis of relative albedo. The Dark subunit is slightly elevated with respect to the Bright materials, and forms a widespread mantle not only in the Lowland valley but elsewhere in the scene. The Bright subunit appears associated with areas of disturbance, such as small craters, ejecta, and steeper sloped areas. A detailed description of the geologic characteristics for each unit is provided in [8].

The valley within Box 1 is mapped primarily as Lowland Bright and Lowland Dark geomorphologic units. Analyses of HiRISE data show that the Dark subunit exhibits greater rock abundance values relative to the Bright. Further, the spatial distribution of the Bright subunit is closely associated with crater ejecta, in particular ejecta from Heimdall crater.

Terrain representative of the Dark subunit is shown in Fig. 3, taken from a HiRISE image at 31 cm/pixel. Organized rock fields are

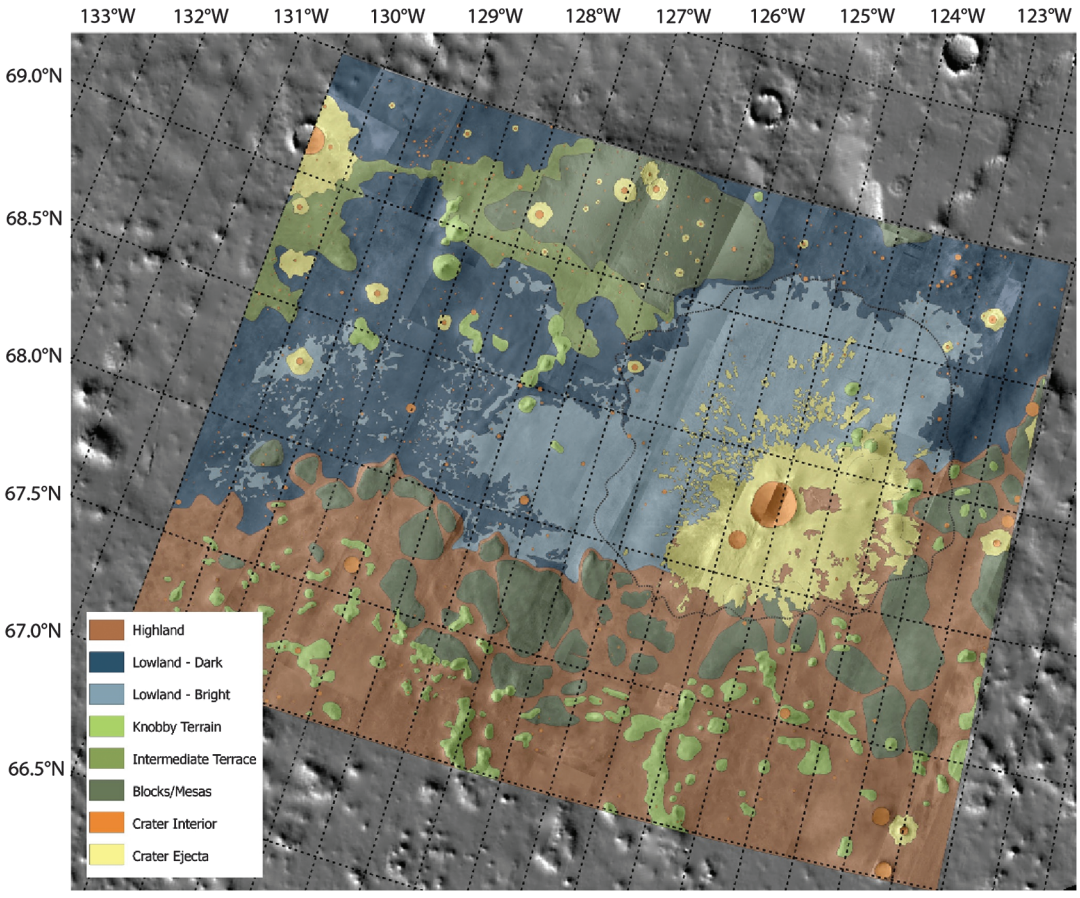

Fig. 2 Geologic map of the candidate landing site, Box 1.

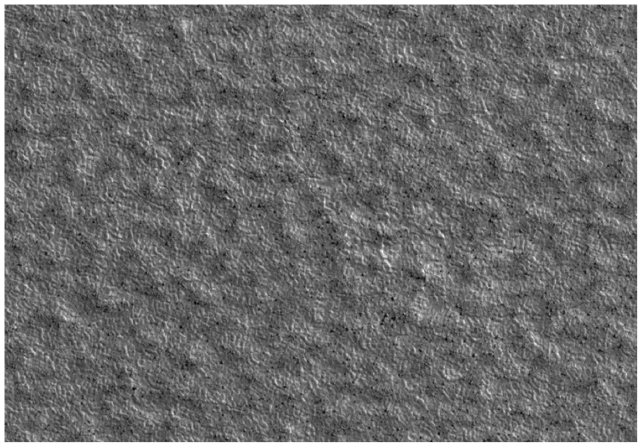

Fig. 3 Organized rock fields representative of Lowland Dark material.

evident throughout the terrain. The mean cumulative fractional area covered by rocks within Fig. 3 is 18%. Figure 4 shows the boundary between the Dark and Bright subunits. The area to the lower right contains the organized rock fields of the Lowland Dark unit, and the upper left contains Lowland Bright material, predominately free of rocks that are greater than 1.5 m in diameter. The correlation between crater ejecta and lower rock abundance as well as the reverse stratigraphic relationship of higher-elevation older terrain are counter-intuitive. The geologic assessment of the landing site concluded that the Lowland Bright subunit represents terrain with low rock abundances and benign slopes. This conclusion formed the basis for the landing ellipse placement as described later in this article.

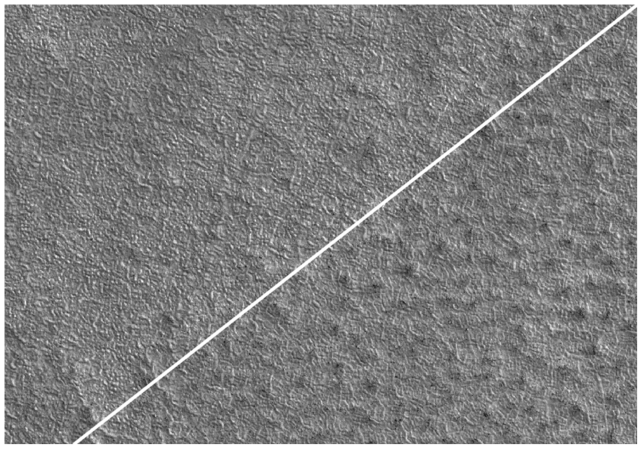

Fig. 4 Unit boundary between Lowland Bright (upper left) and Lowland Dark (lower right) terrains.

Hazard Mapping and Landing Ellipse Placement

With a resolution of 25–31 cm/pixel, HiRISE images make it possible to reliably detect 1.5 m diameter rocks and also to detect many of the rocks 1.0 m and smaller under favorable conditions. HiRISE images were analyzed using a computer algorithm to autocount the diameter, height, and location of rocks based on their shadow dimensions [5]. An example of results from this analysis is shown in Fig. 5. The autocounts were spot checked with hand counts of rocks performed for selected HiRISE images to ensure the quality and accuracy of the counts. Through experience gained in the development of the shadow detection algorithm and observations made of the results, it was determined that the most reliable data were for rocks that had diameters of at least 1.5 m.

Rock size/frequency relationships [9,10] were used to extrapolate from the observable population of large rocks to the full cumulative fractional area (CFA) of rock coverage. The presence of rocks smaller than 1.5 m is estimated using this exponential model, which is based on surface observations made at the two Viking lander sites and the Mars Pathfinder site. An example of this extrapolation from the Viking Lander 2 (VL-2) landing site is shown in Fig. 6, which includes the VL-2 surface observations, three different HiRISE autocounts, and a HiRISE hand count. All five sets of data are consistent with the exponential model curves and support the model's use in extrapolating to smaller diameters. Note the roll off of the hand and autocounts near 1.5 m as the image resolution begins to limit the ability to detect rocks.

Rock CFA statistical distributions for each geomorphic unit (as shown in Fig. 2) were derived from the HiRISE image autocounts. For areas within the Box 1 landing region where no HiRISE coverage was available, the CFA distributions for similar geomorphic units derived from HiRISE autocounts were applied. This approach allowed the rock populations for the entire landing region to be modeled based upon representative HiRISE data.

To evaluate the probability of a catastrophic failure due to rock impact during the landing event or a degraded surface mission due to solar array impingement upon a rock during deployment, a Monte Carlo analysis was developed to simulate Phoenix landing in randomly generated rock fields for a specified range of CFAs [1]. For the purpose of this analysis, rocks were assumed to be hemispherical with a height-to-diameter ratio of 0.5. This height-to-diameter ratio has proven to be a conservative approximation of the surface and orbital observations of Martian rocks. A simulated lander was then randomly placed in these rock fields and checked for contact: first, rock contacts with the three 0.29 m diameter lander footpads were detected and the lander tilt was calculated accordingly, and then the solar array and lander body volumes were checked for interferences to both the rocks and the surface (assumed to be locally flat). The 1.2 m diameter lander body and 1.8 m diameter solar arrays were nominally 0.53 m and 0.70 m above the surface, respectively. Lander placement within rock fields with CFAs ranging from 10 to 30% and surface slopes based upon a digital elevation map of the region ([12])

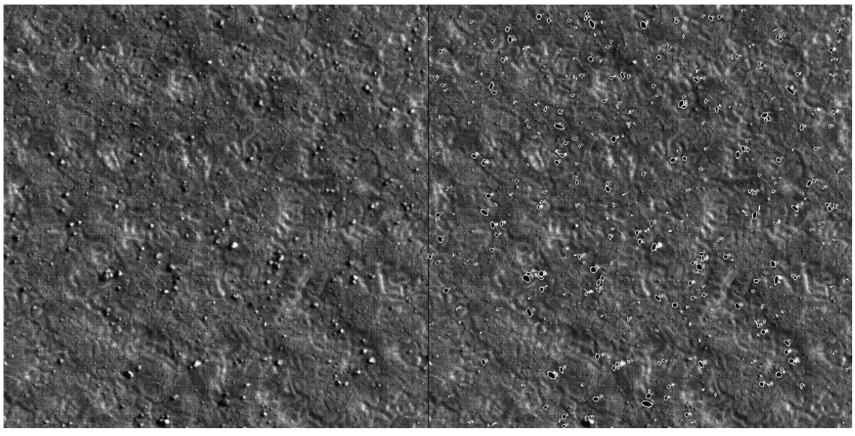

Fig. 5 Example results from the auto rock detection algorithm: a) original HiRISE image, and b) processed image showing identified rock shadows.

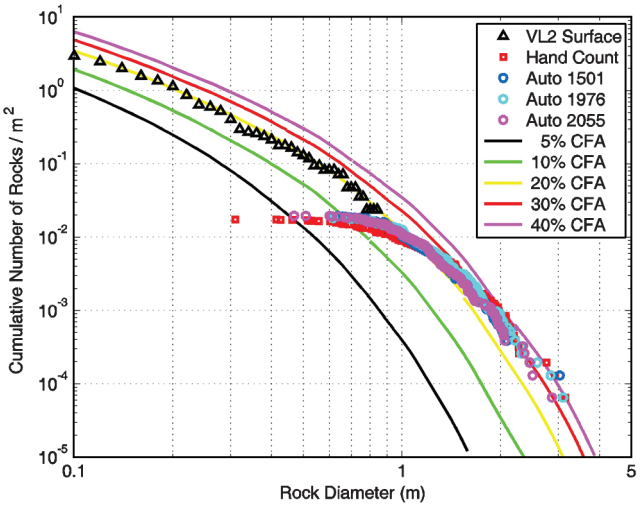

Fig. 6 VL-2 rock counts taken from lander surface images compared with autocounts from three different HiRISE images (PSP_1501, 1976, 2055) and a hand count of PSP_1501, with reference exponential rock model curves at 5, 10, 20, 30, and 40% CFA.

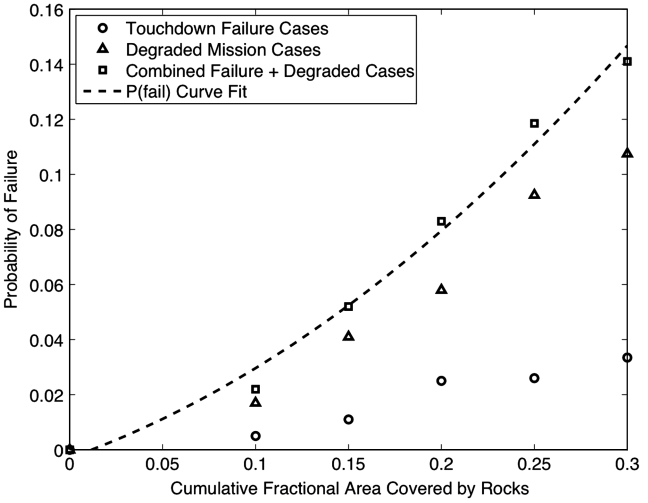

Fig. 7 Probability of failure or degraded mission due to contact with rocks as a function of CFA.

were simulated. Figure 7 shows the resulting probability of mission failure at touchdown due to tipover and rock impact, as well as the probability of a degraded surface mission due to geometrically inhibited solar array deployment. The combined probability p (representing the probability of having a failed or degraded mission due to terrain interaction upon landing) was curve fit with respect to rock CFA, resulting in Eq. (1)

$$p = 0.8667 * \mathrm{CFA}^2 + 0.239 * \mathrm{CFA} - 2.917 \times 10^{-3} \qquad (1)$$

The resulting probabilities, representing landing risk, are shown in the right column of Table 1. Note that in Table 1 the minimum rock count allowed was one rock of diameter 1.5 m per hectare, corresponding to a CFA of 7%. This lower limit was imposed for conservatism, as rocks smaller than 1.5 m could not be reliably detected. Discontinuities in the probability of failed or degraded mission in Table 1 are due to the discretized rock counts. Colors representing the risk levels for four different ranges of CFAs were assigned, allowing the creation of a hazard map as shown in Fig. 8. The green area in Fig. 8 represents the safest landing terrain, providing a basis for landing ellipse placement.

The hazard map in Fig. 8 was used to estimate the overall probability of landing risk due to rocks through convolving the risk associated with rock distributions within each hectare (a hectare is a unit of area equal to 10, 000 m^2) with the statistical probability of landing in that hectare given the landing ellipse placement. This process, described fully by Bonfiglio et al. [11], allowed the determination of the optimal placement of the landing ellipse within

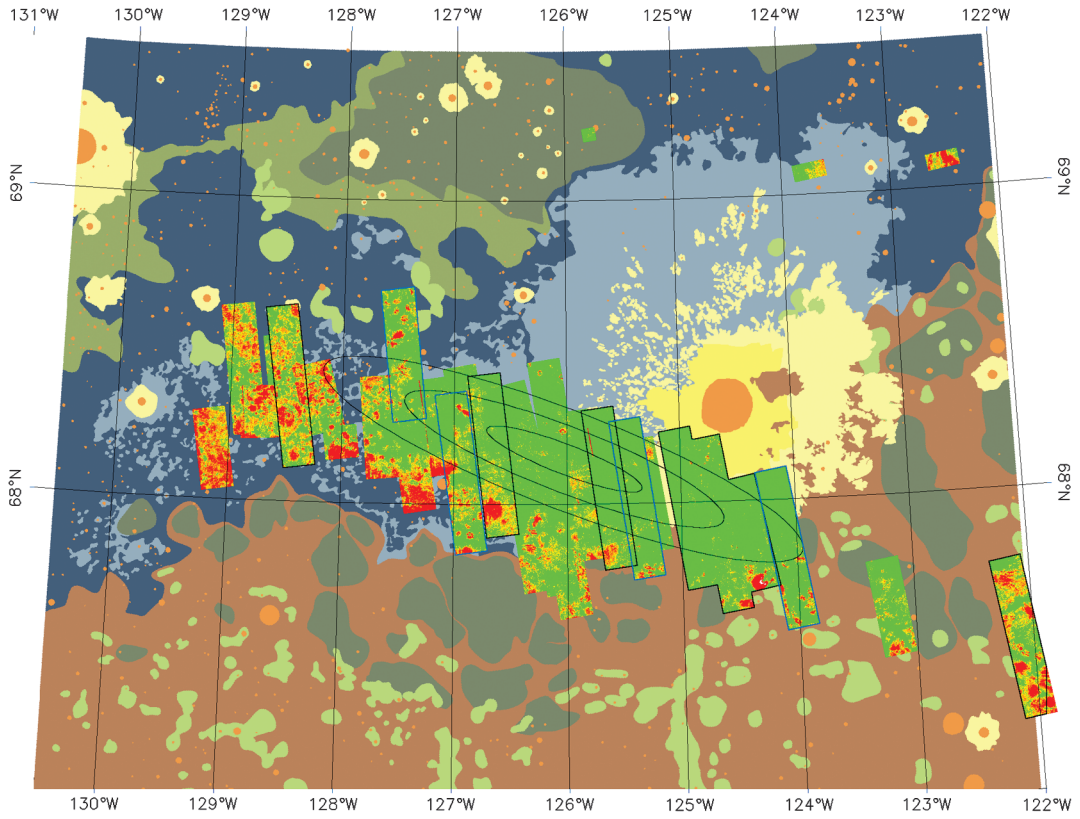

Fig. 8 Landing hazard map for Box 1 with four-color shading applied to HiRISE image locations based upon automated rock counts.

Table 1 Hazard map (Fig. 8) color assignments based upon rock distributions and probability of rock impact

Color	Rocks ≥ 1.5 m Diameter per Hectare	Cumulative fractional area covered by rocks	Probability of failed or degraded mission
Green	1–3	7–10%	0–2.99%
Yellow	4–8	10–14%	3.41–4.88%
Orange	9–19	14–21%	5.23–8.56%
Red	>19	>21%	>8.56%

Box 1; the optimal ellipse placement maximized the probability of a safe landing with respect to terrain hazards. Ellipses representing the one-sigma, two-sigma, and three-sigma landing position uncertainties about the central coordinates are shown. The central coordinates of the landing ellipse were specified as 68.151°N areocentric latitude, 126.025°W longitude. The dimensions of the 99-centile landing ellipse were determined via Monte Carlo simulation to be 100 km × 20 km with the major axis aligned along an azimuth of 111 deg. The landing ellipse major axis aligns with the downtrack direction of the vehicle's entry trajectory. The 99-centile landing ellipse was defined to encompass 99% of the landing locations from the statistical entry, descent, and landing (EDL) Monte Carlo analysis. The probability of a safe landing and subsequent solar array deployment with this ellipse placement was estimated to be 0.98, assuming that the EDL system performed as designed.

Following the Phoenix landing on 25 May 2008, lander localization and HiRISE imaging determined that the touchdown site is at 68.219°N, 234.248°E, as shown in Fig. 9. During the hazard assessment process, the local terrain encompassing this site was estimated to have rock cumulative fractional areas of less than 10%. Quantitative assessment of the rock abundance at the Phoenix landing site is in work by Golombek. Qualitatively, as seen in Fig. 10, the terrain captured by the Phoenix stereoscopic imager is generally free of rocks that would pose a threat to the landing system, consistent with predictions [10].

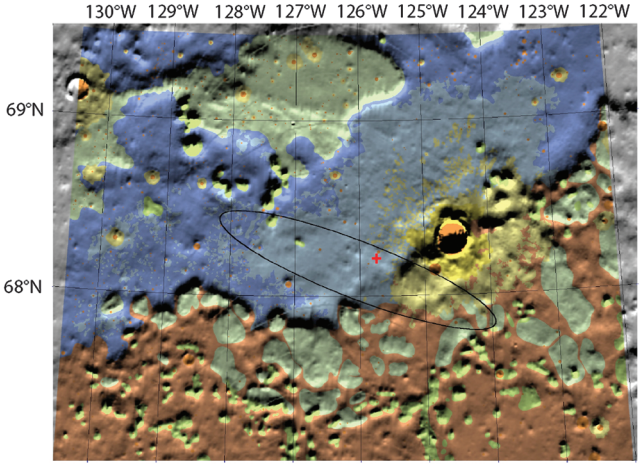

Fig. 9 Phoenix final landing ellipse placement based upon risk assessment (actual Phoenix landing site is indicated by the plus sign).

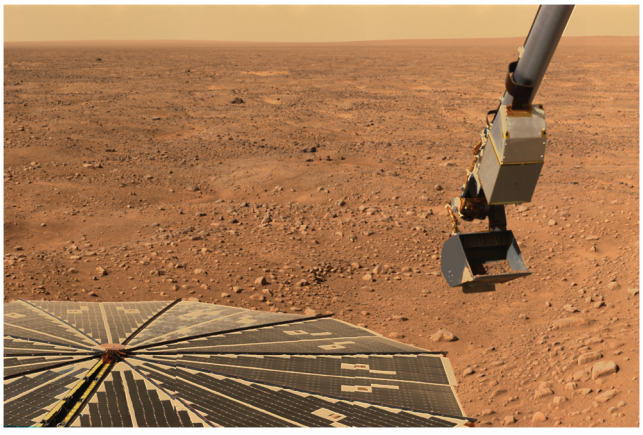

Fig. 10 Landing site panorama taken by Phoenix stereoscopic imager.

Conclusions

The Phoenix landing site hazard assessment and selection process introduced two new elements representing advancements over previous landing site selection processes: the incorporation of images from the MRO HiRISE at 31 cm/pixel, and the utilization of an autonomous rock-counting algorithm that allowed direct identification of potential landing hazards within the areas covered by high-resolution imaging.

Targeted high-resolution images were instrumental in refining the interpretation of the existing lower-resolution thermal and visible imaging data sets, allowing a detailed geologic map to be developed across Box 1. The geologic units within Box 1 were characterized through terrain features, slopes, and rock abundance. This characterization allowed the identification of the Lowland Bright subunit as the preferred terrain for landing ellipse placement, due to low rock abundances and benign slopes.

The automated processing of high-resolution images within Box 1 allowed individual large rocks (1.5 m in diameter or larger) to be counted. Established rock size-frequency distributions provided the mechanism to extrapolate from the autocounts to smaller rock sizes, allowing an inventory of the hazardous rock distributions across the landing footprint. A landing risk assessment was conducted considering scenarios that could result in mission failure or degradation due to lander and solar array interaction with rocks and slopes. The probability of safe landing and subsequent solar array deployment with the selected ellipse placement was estimated to be 0.98, assuming that the EDL system performed as designed.

The local terrain encompassing the Phoenix landing site was predicted to have a rock cumulative fractional area of less than 10%. Following a successful landing on 25 May 2008, images from the Phoenix stereoscopic imager show a landing site generally devoid of hazardous rocks and slopes, consistent with predictions.

Acknowledgments

The authors would like to acknowledge the contributions of Peter Smith, Leslie Tamppari, and Joseph Guinn for their leadership and guidance in the Phoenix landing site selection process. Timothy Parker, Thomas Stein, Selby Cull, and Tabatha Heet made major contributions to the landing site assessment and mapping, and were contributors to this article. Andres Huertas and Yang Cheng were instrumental in the development and utilization of autonomous rock-counting computational tools. Numerous other members of the Phoenix Landing Site Working Group contributed to the work described herein.

References

[1] Adams, D. S., "Phoenix Mars Scout Landing Risk Assessment," *2008 IEEE Aerospace Conference*, IEEE Publications, Piscataway, NJ, 1–8 March 2008. doi:10:1109/AERO.2008.4526286

[2] Grant, J. A., Golombek, M. P., Parker, T. J., Crisp, J. A., Squyres, S. W., and Weitz, C. M., "Selecting Landing Sites for the 2003 Mars Exploration Rovers," *Planetary and Space Science*, Vol. 52, Nos. 1–3, 2004, pp. 11–21. doi:10.1016/j.pss.2003.08.011

[3] Guinn, J. R., Garcia, M. D., and Talley, K., "Mission Design of the Phoenix Mars Scout Mission," *Journal of Geophysical Research*, Vol. 113, No. E00A26. doi:10.1029/2007JE003038

[4] Arvidson, R., Adams, D., Bonifiglio, G., Christensen, P., Cull, S., Golombek, M., Guinn, J., Guinness, E., Heet, T., Kirk, R., Knudson, A., Mellon, M., McEwen, A., Mushkin, A., Parker, T., Seelos IV, F., Seelos,

K., Smith, P., Spencer, D., Stein, T., and Tamppari, L., "Mars Exploration Program 2007 Phoenix Landing Site Selection and Characteristics," *Journal of Geophysical Research*, Vol. 113, No. E00A03, 2008.
doi:10.1029/2007JE003021

[5] Golombek, M. P., Huertas, A., Marlow, J., McGrane, B., Klein, C., Martinez, M., Arvidson, R. E., Heet, T., Barry, L., Seelos, K., Adams, D., Li, W., Matijevic, J. R., Parker, T., Sizemore, H. G., Mellon, M., McEwen, A. S., Tamppari, L. K., and Cheng, Y., "Size-Frequency Distributions of Rocks on the Northern Plains of Mars with Special Reference to Phoenix Landing Surfaces," *Journal of Geophysical Research*, Vol. 113, No. E00A09, 2008.
doi:10.1029/2007JE003065

[6] Tanaka, K. L., Skinner, J. A., and Hare, T. M., "Geologic Map of the Northern Plains of Mars," U.S. Geological Survey Scientific Investigations Map 2888, 2005.

[7] Smith, D. E., Zuber, M. T., Frey, H. V., Garvin, J. B., Head, J. W., Muhleman, D. O., Pettengill, R. J., Solomon, S. C., Zwally, H. J., and Banerdt, W. B., "Topography of the Northern Hemisphere of Mars from the Mars Orbiter Laser Altimeter," *Science*, Vol. 279, No. 5357, 1998, pp. 1686–1692.
doi:10.1126/science.279.5357.1686

[8] Seelos, K. D., Arvidson, R. E., Cull, S. C., Hash, C. D., Heet, T. L., Guinness, E. A., McGuire, P. C., Morris, R. V., Murchie, S. L., Parker, T. J., Roush, T. L., Seelos, F. P., and Wolff, M. J., "Geormorphologic and Mineralogic Characterization of the Northern Plains of Mars at the Phoenix Mission Candidate Landing Sites," *Journal of Geophysical Research*, Vol. 113, No. E00A13, 2008.
doi:10.1029/2008JE003088

[9] Golombek, M., and Rapp, D., "Size-Frequency Distributions of Rocks on Mars and Earth Analog Sites: Implications for Future Landed Missions," *Journal of Geophysical Research*, Vol. 102, 1997, pp. 4117–4129.
doi:10.1029/96JE03319

[10] Golombek, M. P., Haldemann, A. F. C., Forsberg–Taylor, N. K., DiMaggio, E. N., Schroeder, R. D., Jakosky, B. M., Mellon, M. T., and Matijevic, J. R., "Rock Size-Frequency Distributions on Mars and Implications for MER Landing Safety and Operations," *Journal of Geophysical Research*, Vol. 108(E12), No. 8086, 2003, p. 23.
doi:10.1029/2002JE002035

[11] Kirk, R. L., Howington–Kraus, E., Rosiek, M. R., Anderson, J. A., Archinal, B. A., Becker, K. J., Cook, D. A., Galuszka, D. M., Geissler, P. E., Hare, T. M., Holmberg, I. M., Keszthelyi, L. P., Redding, B. L., Delamere, W. A., Gallagher, D., Chapel, J. D., Eliason, E. M., King, R., and McEwen, A. S., "Ultrahigh Resolution Topographic Mapping of Mars with MRO HiRISE Stereo Images: Meter-Scale Slopes of Candidate Phoenix Landing Sites," *Journal of Geophysical Research*, Vol. 113, No. E00A24, 2008.
doi:10.1029/2007JE003000

[12] Bonfiglio, E. P., Adams, D., Craig, L., Spencer, D. A., Strauss, W., Seelos, F. P., Seelos, K. D., Arvidson, R., and Heet, T., "Landing Site Dispersion Analysis and Statistical Assessment for the Mars Phoenix Lander," *AIAA/AAS Astrodynamics Specialist Conference and Exhibit*, AIAA Paper 2008-7348, Aug. 18–21, 2008.

C. Kluever
Associate Editor